Hyperfine Interact
DOI 10.1007/s10751-012-0643-2

Nuclear resonance vibrational spectroscopy (NRVS) of rubredoxin and MoFe protein crystals

Yisong Guo · Eric Brecht · Kristen Aznavour · Jay C. Nix · Yuming Xiao · Hongxin Wang · Simon J. George · Robert Bau · Stephen Keable · John W. Peters · Michael W. W. Adams · Francis E. Jenney Jr. · Wolfgang Sturhahn · Ercan E. Alp · Jiyong Zhao · Yoshitaka Yoda · Stephen P. Cramer

Abstract We have applied ^{57}Fe nuclear resonance vibrational spectroscopy (NRVS) for the first time to study the dynamics of Fe centers in Iron-sulfur protein crystals, including oxidized wild type rubredoxin crystals from *Pyrococcus furiosus*, and the

Electronic supplementary material The online version of this article (doi:10.1007/s10751-012-0643-2) contains supplementary material, which is available to authorized users.

The UC Davis Department of Applied Science is deceased.

Y. Guo · Y. Xiao · H. Wang · S. P. Cramer
Department of Applied Science, University of California, Davis, CA 95616, USA

E. Brecht · S. Keable · J. W. Peters
Department of Chemistry and Biochemistry, Montana State University, Bozeman, MT 59717, USA

K. Aznavour · R. Bau
Department of Chemistry, University of Southern California, Los Angeles, CA 90089, USA

J. C. Nix · H. Wang · S. J. George · S. P. Cramer (✉)
Physical Biosciences Division, Lawrence Berkeley National Laboratory, Berkeley, CA 94720, USA
e-mail: spcramer@lbl.gov

W. Sturhahn · E. E. Alp · J. Zhao
Advanced Photon Source, Argonne National Laboratory, Argonne, IL 60439, USA

Y. Yoda
JASRI, SPring-8, 1-1-1 Kouto, Sayo-cho, Sayo-gun, Hyogo 679-5198, Japan

M. W. W. Adams
Department of Biochemistry and Molecular Biology, University of Georgia, Athens, GA 30602, USA

F. E. Jenney Jr.
Georgia Campus, Philadelphia College of Osteopathic Medicine, Suwanee, GA 30024, USA

S. P. Cramer
Department of Chemistry, University of California, Davis, CA 95616, USA

Published online: 04 October 2012

MoFe protein of nitrogenase from *Azotobacter vinelandii*. Thanks to the NRVS selection rule, selectively probed vibrational modes have been observed in both oriented rubredoxin and MoFe protein crystals. The NRVS work was complemented by extended X-ray absorption fine structure spectroscopy (EXAFS) measurements on oxidized wild type rubredoxin crystals from *Pyrococcus furiosus*. The EXAFS spectra revealed the Fe-S bond length difference in oxidized *Pf* Rd protein, which is qualitatively consistent with the crystal structure.

Keywords ^{57}Fe · Nuclear resonant scattering · Nuclear resonance vibrational spectroscopy · NRVS · Mössbauer · Synchrotron radiation · EXAFS · Normal mode analysis · Nitrogenase · Rubredoxin

1 Introduction

Iron-sulfur (Fe-S) proteins serve a wide variety of essential tasks in living systems, including electron transfer within and between proteins, catalysis of chemical reactions, sensing the chemical environment, regulation of DNA expression, repair of damaged DNA, and maintenance of molecular structure [1]. The importance of understanding the structure and function of these proteins can hardly be overstated. The synchrotron radiation based methods, EXAFS (Extended X-Ray Absorption Fine Structure) and NRVS (Nuclear Resonance Vibrational Spectroscopy) have both become popular tools for the study of such Fe-S proteins. Although most often used on non-oriented samples, both techniques have an angular dependence that can be employed to extract additional information about a sample. In the case of EXAFS, the modulation χ of the X-ray absorption for atom a due to the presence of backscattering atom b is sensitive to the angle θ between the a-b axis $\vec{R}_{ab}$ and the electric field polarization $\vec{E}$: $\chi \propto 3\cos^2\theta$. In contrast, the nuclear absorption probability S(E) (and the NRVS signal) is sensitive to the ^{57}Fe motion $\vec{e}_\alpha$ in a given normal mode α along the beam propagation direction $\hat{k}$: $\mathrm{S(E)} \propto \left(\hat{k} \bullet \vec{e}_\alpha\right)^2$.

In this paper we report the first single crystal NRVS on two Fe-S proteins—oxidized wild type (WT) rubredoxin from *Pyrococcus furiosus* (*Pf* Rd) and MoFe protein from *Azotobacter vinelandii* (*Av*). We demonstrate how the combined application of EXAFS and NRVS to oriented samples can provide additional information about the dynamics of complex Fe-S sites in metalloproteins. The particular samples chosen represent two extremes of complexity. We start by illustrating single crystal spectroscopy of rubredoxin, the simplest known Fe-S protein, with a single approximately tetrahedral FeS_4 center (Fig. 1). We then illustrate work with nitrogenase, which contains the most complex metal sulfur cluster in biology—the $MoFe_7S_9X$ FeMo cofactor (Fig. 1).

NRVS has rapidly become a popular technique for probing the dynamics of Fe sites in metalloproteins [3–12] as well as Fe containing inorganic complexes [13–24]. NRVS only probes the vibrational modes in which ^{57}Fe nuclei move along the incident beam direction [21, 25, 26]. This unique selection rule makes NRVS free of any interference from solvent and other protein vibrations (which often limit FT-IR spectroscopy) and independent of oxidation states (which often restricts resonance Raman spectroscopy) [5, 7]. For bioinorganic applications, NRVS has been used to probe the dynamics of Fe sites in heme proteins [9–12], Fe-S proteins,

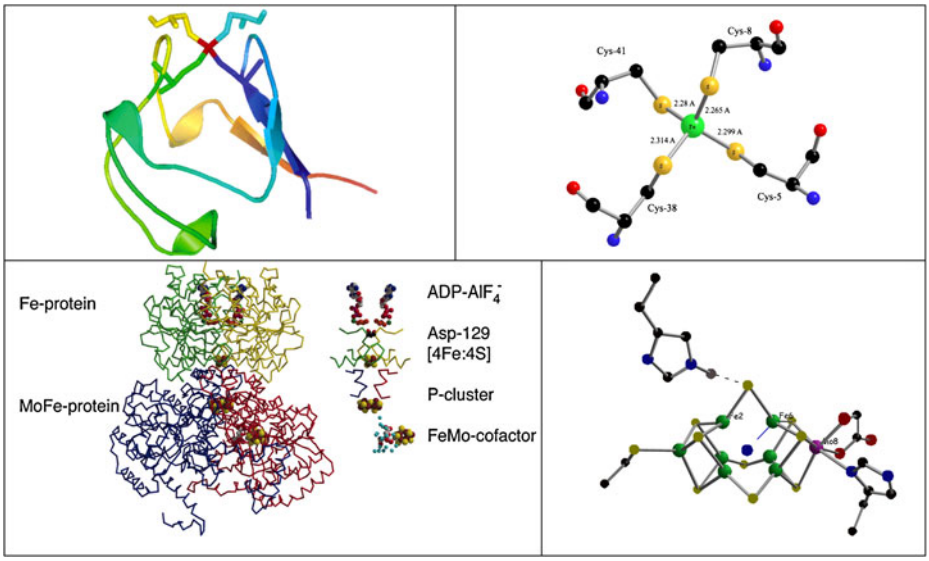

Fig. 1 *Top left*: a cartoon of oxidized *Pf* Rd, including sticks for cysteine residues, illustrating exposed location of Fe site (*red*). *Top right*: close-up of Fe site showing slight compression of Fe-SCys8 and Fe-SCys41 bonds (PDB Code 1BRF) [2]. *Bottom left*: N_2ase MoFe protein. *Bottom right*: close-up of FeMo cofactor

including rubredoxins [5], [2Fe-2S] and [4Fe-4S] ferredoxins [7], hydrogenase [6], and nitrogenase [3]. Previous experiments with orienting crystal samples have been performed on several heme protein related model compound crystals [20–22] to identify in-plane and out-of-plane vibrations with respect to the porphyrin plane.

The details of NRVS theory have been explained in [21, 25, 26], the bottom line for the current study is that a NRVS transition for normal mode α contributes a fraction ϕ_α to the normalized excitation probability $S(\overline{\nu})$ that is directly proportional to the Fe mode composition factor $e^2_{j\alpha}$ and inversely proportional to $\overline{\nu}_\alpha$ [21, 27]:

$$\phi_\alpha = \frac{1}{3}\frac{\overline{\nu}_R}{\overline{\nu}_\alpha} e^2_{j\alpha} \left(\overline{n}_\alpha + 1\right) f \tag{1}$$

In the above equation, $\overline{\nu}_\alpha$ is the difference between the photon energy and the recoil-free nuclear resonance energy in wave numbers, $\overline{\nu}_R$ is the recoil energy ($\sim$16 cm^{-1}), $\overline{n}_\alpha = \left[\exp\left(hc\overline{\nu}_\alpha / k_B T\right) - 1\right]^{-1}$ is the thermal occupation factor for a mode of frequency $\overline{\nu}_\alpha$ at temperature T [21], and the recoilless fraction f depends on $<x^2_{Fe}>$, the mean square fluctuation of the Fe nucleus along the beam direction, via $f = \exp(-k^2 <x^2_{Fe}>)$. The data are often presented as the ^{57}Fe-centered partial vibrational density of states (PVDOS), $D_{Fe}(\overline{\nu})$, using a lineshape function $L(\overline{\nu} - \overline{\nu}_\alpha)$ [18, 21]:

$$D_{Fe}(\overline{\nu}) = \sum_\alpha \left(\hat{k} \bullet \vec{e}_{Fe,\alpha}\right)^2 L(\overline{\nu} - \overline{\nu}_\alpha) \tag{2}$$

The ^{57}Fe PVDOS for measurements on a perfectly oriented sample takes the form of a series of bands with areas $\left(\hat{k} \bullet \vec{e}_{Fe,\alpha}\right)^2$ equal to the squared projection of $e^2_{j\alpha}$ along the beam direction $\hat{k}$.

Rubredoxins are small (~50 amino acids) electron-transfer proteins that contain a single Fe(S-cys)$_4$ redox center [28]. The high-resolution X-ray crystal structure for oxidized *Pyrococcus furiosus* rubredoxin (*Pf* Rd) at 0.95 Å resolution (1BRF) [2] along with several other Rd crystal structures from different bacteria [29, 30] reveals a roughly tetrahedral FeS_4 site, often described as approaching D_{2d} symmetry via a compression along a S_4 axis (Fig. 1). In a previous study, we examined *Pf* Rd containing the unprocessed N-terminal methionine residue (*Pf* met-Rd) in frozen solution sample via NRVS. We observed three broad bands of intensity, near 70, 150, and 360 cm^{-1} [5].

Nitrogenase (N_2ase) is an important enzyme that catalyzes the reduction of dinitrogen (N_2) to ammonia (NH_3) and is ultimately responsible for about half of the food produced globally each year. The Mo version of N_2ase from *Azotobacter vinelandii* consists of two components, the Fe protein (*Av2*) and the MoFe protein (*Av1*). *Av2* contains one [Fe_4S_4] cluster, and (coupled with the hydrolysis of MgATP) transfers electrons to *Av*1. *Av1* is an $\alpha_2\beta_2$ tetramer, and it contains two [Fe_7MoS_9X] FeMo cofactors and two [Fe_8S_7] P clusters. The FeMo cofactor is the active center of N_2ase, and it is the most complicated Fe-S cluster found in biology. In our previous NRVS study [3] of MoFe protein in frozen solution, a unique spectral feature at ~190 cm^{-1} has been observed, which we assigned to FeMo cofactor cluster breathing modes.

2 Experimental section

Rubredoxin crystal sample preparation ^{57}Fe enriched WT *Pf* Rd was prepared at the University of Georgia. The experimental (biological) procedures of obtaining and purifying the sample have been described [31]. In this section, we describe the method we used to obtain the large crystals necessary for the NRVS experiment. "X-ray sized" crystals of ^{57}Fe WT *Pf* Rd were first grown at room temperature using hanging drop method [32] by equilibrating a 4 µl drop against 1 ml of deuterated 3.8 M NaK phosphate solution (equimolar of NaD_2PO_4 and H_2DPO_4) as precipitating agent. The drop contains 2 µl of 40 mg/ml protein solution and 2 µl of the NaK phosphate solution. The small crystals, which appeared in about 3 days, were first collected and crushed, then used as a concentrated seed stock [32]. The concentrated seed stock was then diluted repeatedly with 3.6 M $NaKPO_4$ solution to reduce the concentration. The concentration was reduced 10-fold in each step: 10 µl of the seed stock solution was mixed with 90 µl of the 3.6 M $NaKPO_4$ solution and the step was repeated 3 times so that there was a minimal amount of crystal seeds in each drop of the solution. The seed thus serves as a template on which further molecules can assemble, and with time the seed can grow into a large crystal. In order to obtain large, 1 mm^3-sized crystals, the sitting drop method [32] was used by equilibrating 30 or 40 µl of a mixture of protein and crystallization agent (3:1 and 4:1 ratio) against 1 ml of 3.8 NaK phosphate solution. 0.2 µl of the seed stock of the rubredoxin solution was added to seed the sample. If more than one crystal is formed within the sitting drop, a small amount of D_2O is used to dissolve most of the crystals, allowing only

one crystal per drop to grow. The crystal size used in our experiments is ~0.5–1 mm^3, however, using the method described above, crystals can be grown up to ~4 mm^3 in the period of 3 months. The crystals were stabilized during growth by increasing the concentration of the reservoir solution from 3.8 M to 4.0 M.

MoFe protein sample preparation The MoFe protein was concentrated to ~60 mg/ml as determined by Bradford assay. MoFe protein crystals were grown under nitrogen atmosphere in a Braun chamber by microcapillary batch diffusion [33]. The precipitating solutions consisted of 30 % PEG 4000, 100 mM Tris (pH 8.0), and 150–200 mM Na_2MoO_4. The MoFe crystals were observed to have a dark brown color and grow to the desired size for data collection within 1–2 months. Crystals were harvested on rayon loops and flash cooled in liquid nitrogen.

Crystal orientation Oxidized *Pf* Rd crystals were oriented at Beamline 4.2.2 at the Advanced Light Source (ALS). Crystals were first transferred onto plastic cryo-loops from mother liquid, flash frozen in liquid nitrogen, then placed onto an x-ray diffractometer to find crystal axes. For NRVS samples, the crystal *a*-axis or *c*-axis was aligned along incident x-ray direction; for EXAFS samples, the crystal *a*-axis or *c*-axis were aligned parallel to the x-ray polarization direction. Aligned crystals were transferred onto custom made Lucite disc cells in liquid nitrogen. The crystals used ranged from 0.5 to 1 mm^3, flash freezing crystals of this size did not noticeably crack the crystals, and good quality diffraction pattern can still be obtained. Figure S3 shows the oriented crystal placed in the custom made Lucite NRVS disc cells and the diffraction pattern obtained from this crystal.

Nuclear resonance vibrational spectroscopy ^{57}Fe NRVS data were recorded using published procedures [26] on multiple occasions at Beamline 3-ID at the Advanced Photon Source (APS) [34] and BL09XU at SPring-8, Japan [35]. Beamline 3-ID provided ~2.5×10^9 photons/sec in 1 meV bandwidth at 14.4125 keV in a 1 mm (vertical) × 3 mm (horizontal) spot, using a water-cooled diamond (1,1,1) double crystal monochromator with 1.1 eV bandpass, followed by separate Si(4,0,0) and Si(10,6,4) channel-cut crystals in a symmetric geometry. The flux at SPring-8 was ~3×10^9 in a 1.1 meV bandwidth, using a LN_2-cooled Si(1,1,1) double crystal monochromator followed by asymmetrically cut Ge(4,2,2) and two Si(9,7,5) crystals. During these measurements, crystal samples were maintained at low temperatures using liquid He cryostats. Temperatures were calculated using the ratio of anti-Stokes to Stokes intensity according to: $S(-E) = S(E)\exp(-E/kT)$. Spectra were recorded between −20 meV and 80 meV in 0.25 meV step at APS and 0.3 meV step at SPring-8. Delayed nuclear fluorescence and Fe K fluorescence were recorded with a single 1 cm^2 square avalanche photodiode (APD) at the APS and with an APD array at SPring-8. Each scan took about 40 min, and all scans were added and normalized to the intensity of the incident beam.

X-ray absorption spectroscopy Fe K-edge x-ray absorption data were measured at Stanford Synchrotron Radiation Laboratory beamline 9–3, with a Si 220 double-crystal monochromator and two Rh-coated mirrors: one flat premonochromator mirror for harmonic rejection and vertical collimation and one toroidal postmonochromator mirror for focusing. Fluorescent x-rays were measured using a 30-element Ge fluorescence detector (Canberra Industries), fitted with Soller slits to minimize

the relative contribution of scattered radiation. An Oxford Instruments CF1208 liquid He cooled sample cryostat was used to maintain the sample temperature at 9 K. The x-ray energy was calibrated using the first inflection point of a standard Fe foil set as 7112 eV. This was measured at the same time as the sample spectrum using two ion chambers positioned downstream of the cryostat. To minimize x-ray photoreduction, the sample was moved after each scan so that the beam irradiated a different spot on the sample for each scan—typically two spots were available for each crystal and 3∼5 scans were collected requiring reuse of each spot. In addition to that, Al foils were used in front of the incident beam ion chamber to reduce the flux of the incident x-ray beam. The Fe K-edge structure and position were monitored to ensure that no significant photochemistry had occurred.

Normal mode calculations The normal mode calculations were carried out on structural models derived from crystallographic coordinates. A modification of program "VIBRATZ" was used to calculate the normal modes and NRVS spectra [36, 37], using Wilson's GF matrix method and a Urey-Bradley force field. A QR algorithm was used for finding eigenvectors [38]. The NRVS spectra obtained from different orientations were optimized simultaneously.

EXAFS data analysis EXAFS data were analyzed using the EXAFSPAK software suite [39]. As the samples contained no glassing agent, it was first necessary to rigorously screen the data from the individual detector elements to eliminate any diffraction artifacts. Curve fitting used the EXAFSPAK program OPT, with single-scattering phase and amplitude functions calculated using FEFF 7.0 [40].

3 Results and discussion

3.1 XANES and EXAFS on oxidized *Pf* Rd crystals

We begin by presenting single crystal EXAFS measurements on the same ^{57}Fe-enriched *Pf* Rd crystals as used for the NRVS work, because the results complement and help interpret the latter experiment. The high-resolution x-ray crystal structure for oxidized *Pf* Rd at 0.95 Å resolution (1BRF) shows that there are 4 Rd molecules in each crystal unit cell [2]. The Fe-S bonds connected to Cys5 and Cys38 lie close to the *bc* plane of the crystal with a larger projection onto the *c*-axis, while the Fe-S bonds involving Cys8 and Cys41 are closer to the *ab* plane with a larger projection onto the *a*-axis. Thus, by aligning the x-ray polarization direction along the *a*-axis ($\vec{E}||\vec{a}$), the x-ray absorption will mainly probe along the Fe-S bonds for Fe-SCys8 and Fe-SCys41, while with the x-ray polarization along the *c*-axis ($\vec{E}||\vec{c}$), the XANES and EXAFS will be more selective for the Fe-S bonds associated with Fe-SCys5 and Fe-SCys38.

The Fe K-edge spectra for Rd crystals with $\vec{E}||\vec{a}$ and $\vec{E}||\vec{c}$ are shown in Fig. 2. Both spectra have similar features with a strong $1s \rightarrow 3d$ peak at ∼7112.8 eV and a shoulder at ∼7119.8 eV, consistent with previous studies on Rd solution samples [24, 25]. The strength of the pre-edge features in both spectra arises from mixing of *d* and *p* orbitals in the roughly tetrahedral Fe site geometry. The slight intensity difference of the pre-edge features in $\vec{E}||\vec{a}$ and $\vec{E}||\vec{c}$ spectra may come from a slightly different degree of mixing for different orientations.

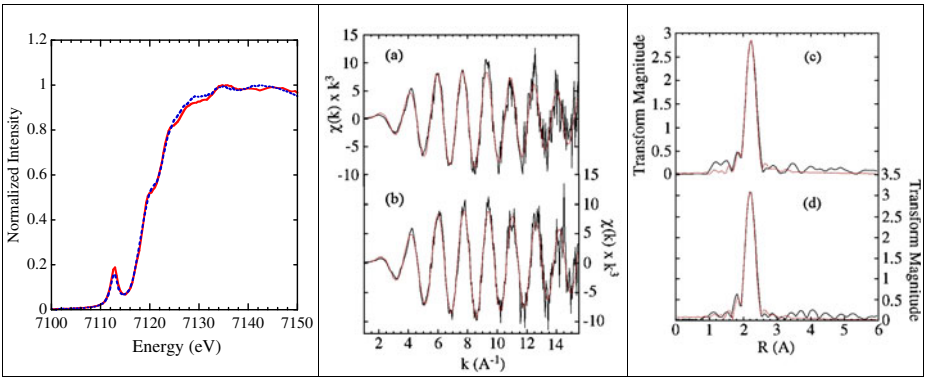

Fig. 2 Single crystal XANES and EXAFS. *Left*: Fe K-edge of the *Pf* Rd crystals with $\vec{E}||\vec{a}$ (*blue dotted line*) and $\vec{E}||\vec{c}$ (*red solid line*). *Middle*: k^3-weighted EXAFS of the oxidized *Pf* Rd with $\vec{E}||\vec{a}$ (b) vs. $\vec{E}||\vec{c}$ (a). *Right*: EXAFS Fourier transforms for $\vec{E}||\vec{a}$ (d) vs. $\vec{E}||$c(c)

Figure 2 also presents the EXAFS spectra and Fourier transform for crystals with $\vec{E}||\vec{a}$ and $\vec{E}||\vec{c}$ together with representative fits. The fitting parameters are listed in Table S1. The Fourier transforms of the EXAFS spectra reveal a single Fe-S peak at ~2.25–2.30 Å from the Fe-SCys interactions. For the $\vec{E}||\vec{a}$ spectrum, a fit to the k-space EXAFS gave an Fe-S distance of 2.263 Å, while the $\vec{E}||\vec{c}$ spectrum fit gave a distance of 2.284 Å. The EXAFS results show about the same bond length differential as the x-ray crystal structure, but with slightly shorter average distances. For example, the crystal structure shows that the two shorter (2.273 average) Fe-S bonds (Fe-SCys8, 2.265 Å and Fe-SCys41 2.280 Å) have larger projections onto the *a*-axis, while the two longer (2.307 average) Fe-S bonds (Fe-SCys5, 2. 299 Å and Fe-SCys38, 2.314 Å) have larger projection onto the *c*-axis. The slightly longer average crystallographic Fe-S distance (2.29 Å) may in fact be the result of photoreduction in the diffraction measurement.

3.2 Single crystal NRVS on oxidized *Pf* Rd

NRVS spectra for oxidized *Pf* Rd single crystals are shown in Fig. 3 together with the oxidized Rd in solution [5] from the recombinant rubredoxin containing the unprocessed N-terminal methionine residue (*Pf* met-Rd) [31]. Overall, the crystal spectra exhibit the same three main regions of intensity, near 70, 140, and 360 cm^{-1}, as the solution NRVS. However, the crystal spectra intensities differ from the solution spectrum, especially near 360 cm^{-1}. This is because the single crystal experiment is selecting particular modes from the overall envelope. In the crystal NRVS spectra, the *a*-axis and *c*-axis were aligned along the x-ray beam direction, so that the normal modes with a component of ^{57}Fe motion along the *a*-axis or *c*-axis are enhanced.

In previous NRVS studies on oxidized *Pf* met-Rd, the 360 cm^{-1} region, which had significant intensity in an envelope between 345 and 375 cm^{-1}, was assigned to asymmetric Fe-S stretching modes. In this region, clear intensity differences can be seen for spectra from different crystal orientations. The $\hat{k}||\vec{a}$ PVDOS shows one strong peak at 373 cm^{-1} with two lower energy shoulders at ~360 cm^{-1} and

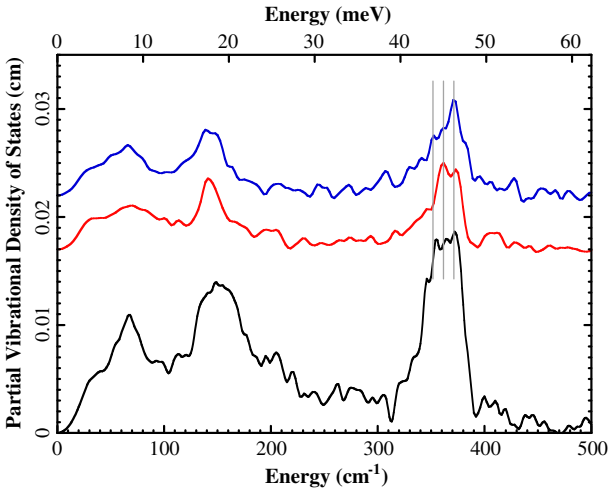

Fig. 3 ^{57}Fe PVDOS for top: oxidized Pf Rd with $\hat{k}||\vec{c}$ (*red line*) or $\hat{k}||\vec{a}$ (*blue line*) and bottom: oxidized *Pf* met-Rd in solution form (5)

$\sim$350 cm^{-1}, while in the $\hat{k}||\vec{c}$ spectrum, the 360 cm^{-1} shoulder in becomes the strongest peak in this region, the intensity of 373 cm^{-1} peak decreases and 350 cm^{-1} shoulder disappears. These three features are consistent with the three asymmetric Fe-S stretching modes assigned at 375, 358 and 350 cm^{-1} in the previous study [5]. The intensity differences of the same peaks in different crystal orientations indicate that the ^{57}Fe motions in these vibrational modes have preferred orientations.

In the bending region (100 $\sim$ 200 cm^{-1}), the $\hat{k}||\vec{a}$ and $\hat{k}||\vec{c}$ NRVS spectra show similar features with a strong peak at $\sim$140 cm^{-1}; in the $\hat{k}||\vec{a}$ orientation this peak is slightly split. Both orientations lose intensity in the region between 155 cm^{-1} and 220 cm^{-1} compared with the solution Rd spectrum. This indicates that ^{57}Fe motion in vibrational modes of this region have less projection onto the *a*- and *c*-axes. However, detailed analysis of this bending region and the region below 100 cm^{-1} of the crystal spectra is beyond the scope of this work.

For a more quantitative interpretation, we built a simple Fe(SCC)$_4$ model with no symmetry constraints, using the Fe site geometry from the oxidized WT *Pf* Rd crystal structure. We used force constants from a previous Fe(SCC)$_4$ simulation of solution *Pf* met-Rd NRVS as a starting point [5]. The three spectra, oxidized solution *Pf* met-Rd NRVS, $\hat{k}||\vec{a}$ and $\hat{k}||\vec{c}$ WT *Pf* Rd crystal NRVS, were simultaneously modeled by least squares fitting. (We assume that the oxidized WT *Pf* Rd NRVS in solution form should be very similar to the oxidized *Pf* met-Rd NRVS in solution form, at least in the Fe-S stretch region, because of their almost identical Fe site geometry). Since the NRVS intensity below 200 cm^{-1} involves contributions from cysteine side chain vibrations and motion of the protein backbone in Rd NRVS spectra [5] our Fe(SCC)$_4$ model is too small to capture those features. So, here we focus on the Fe-S stretch region by fixing bending force constants to those for the previous oxidized *Pf* met-Rd NRVS simulation.

Figure 4 shows the simulations for the crystal spectra. The $\hat{k}||\vec{a}$ simulation shows two Fe-S stretching modes at 357 and 373 cm^{-1}, and the relative intensities are consistent with the experimental data. The 352 cm^{-1} mode simulated in the solution spectrum has almost disappeared, indicating that the Fe motion in this mode is almost

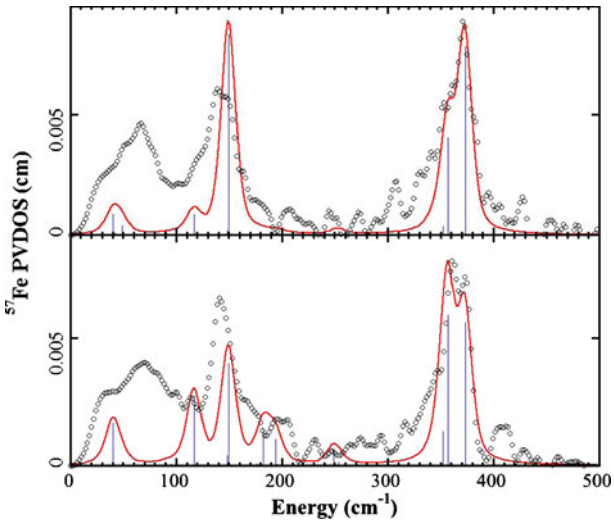

Fig. 4 ^{57}Fe PVDOS of *Pf* Rd crystal data (∘ ∘ ∘) and simulations using $Fe(SCC)_4$ model from 1BRF crystal structure. *Sticks* represent intensities of individual normal modes. *Top*: $\hat{k}||\vec{a}$. *Bottom*: $\hat{k}||\vec{c}$. Scale reduction factors of 1.48 for $\hat{k}||\vec{a}$ and 1.38 for $\hat{k}||\vec{c}$ were used

perpendicular to the crystal *a* axis. In the $\hat{k}||\vec{c}$ simulation, the relative intensities of the modes at 357 and 373 cm^{-1} are inverted, also consistent with the experimental data. The bottom line is satisfying if not surprising: the highest frequency mode (373 cm^{-1}) has the most intensity in the direction with the shorter (2.263 Å) average Fe-S bond length, while the lower frequency modes are stronger along the longer (2.284 Å) average Fe-S bonds.

Clearly there are additional features in the experimental spectra that are not captured in the bare-bones simulations. Work is being pursued with more complex $Fe(S\text{-}cysX_5)_4$ models, in which the remaining cysteine atoms are added, as well as the carbonyl C and O of the residue adjacent to the cysteine N, and the amide N of the residue bound to the cysteine carbonyl group.

3.3 NRVS on nitrogenase MoFe protein crystals

Figure 5 shows the NRVS for a MoFe protein crystal with the *c*-axis aligned along the incident x-ray direction (referred to as $\hat{k}||\vec{c}$ from now on), and the NRVS obtained for the same crystal by turning the sample cell 90° (referred to as $\hat{k} \perp \vec{c}$). The sample we used was actually a multi-crystal containing more than one single crystal, the crystal axes of these sub-crystals were roughly aligned with each other. The crystal size was ~0.5-0.7 mm^3. Although the statistics and alignment are limited for these preliminary data, we nevertheless observe clear intensity differences for features between 50 and 250 cm^{-1}. (Because of the limited statistics of the current spectra, we do not discuss the region above 250 cm^{-1}.)

In the $\hat{k} \perp \vec{c}$ NRVS, there is an overall maximum at 188 cm^{-1}, a shoulder at 177 cm^{-1}, and a lesser peak at 148 cm^{-1}. In contrast, the $\hat{k}||\vec{c}$ NRVS shows a decrease in the 188 cm^{-1} peak and increased intensity for the 148 cm^{-1} peak. The feature at 177 cm^{-1} also becomes clearly resolved. Another clear difference is at ~84 cm^{-1}, where a distinct peak is seen in the $\hat{k}||\vec{c}$ spectrum, while in the $\hat{k}\perp\vec{c}$ spectrum, this feature disappears. Finally, both spectra have a higher energy shoulder observed at

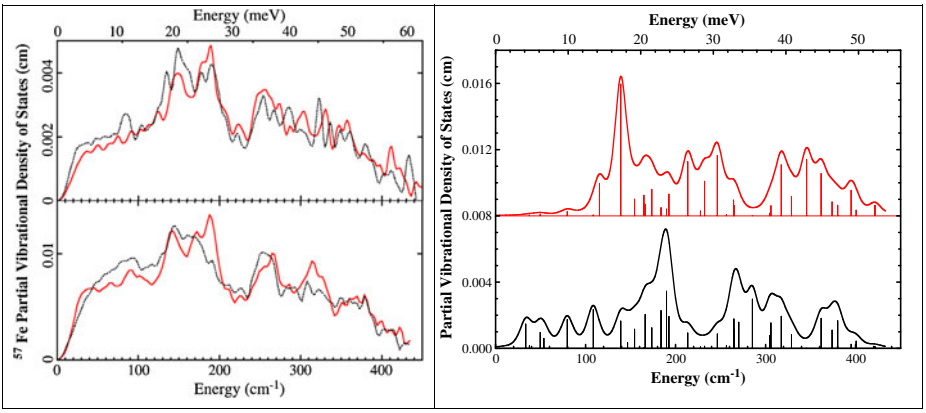

Fig. 5 *Left, top*: ^{57}Fe PVDOS for MoFe protein crystal with $\hat{k}||\vec{c}$ (*black dashed line*) and $\hat{k} \perp \vec{c}$ (*red line*). *Left, bottom*: MoFe protein in solution (*red line*) and P-cluster in Δ*nif*E MoFe protein (*black dashed line*). *Right*: Calculated ^{57}Fe PVDOS of FeMo cofactor assuming the C_3 axis is parallel to the incident x-ray direction (*top*) and perpendicular to the incident x-ray direction (*bottom*). *Sticks* represent intensities of individual normal modes

206 cm^{-1} and another apparent band at ∼225 cm^{-1}. Overall, the changes in band intensities prove that the ^{57}Fe nuclear motions in the vibrational modes of this region have preferred directions.

In our previous NRVS study [3], the NRVS spectra of both wild type MoFe protein (*Av1*) and a Δ*nif*E mutant protein (Δ*nif*E:*Av1*) that only contains P-clusters were reported (Fig. 5). The unique feature in the *Av1* spectrum compared with the Δ*nif*E:*Av1* spectrum was the peak at ∼190 cm^{-1} with a lower energy shoulder at ∼175 cm^{-1}. This feature therefore must belong to a vibrational mode of the FeMo cofactor in MoFe protein.

Previously, a C_{3v} symmetry $[O_3MoFe_7NS_9(SC)]^{n-}$ model was used to successfully simulate the FeMo cofactor spectrum [3]. Five normal modes, including 2 A_1 modes and 3 E modes, were assigned to the region between 160 and 200 cm^{-1}, and a strong E mode was assigned to the peak at 141 cm^{-1}. Inspection of the five normal modes between 160 and 200 cm^{-1} shows that the directions of the Fe motions in these modes are closer to the plane perpendicular to the C_3 symmetry axis (the line formed by the capping Mo and Fe atoms) than along this axis, while for the E mode at 141 cm^{-1}, the Fe motions are more along the C_3 symmetry axis (Fig. 6). Figure 5 shows the predicted NRVS spectra of assuming molecular C_3 axis parallel to the incident X-ray or perpendicular to the incident X-ray.

By inspecting the crystal structure of MoFe protein, we found that the crystal *b*-axis is roughly perpendicular to the C_3 symmetry axis of the FeMo-co, and the crystal *a*- or *c*- axis is roughly parallel to the C_3 axis (Figure S3). In our crystal MoFe protein NRVS experiments, due to the experimental setup limitation, the two crystal orientations we selected actually were $\hat{k}||\vec{c}$ and $\hat{k}\perp\vec{c}$, instead of exact $\hat{k}||\vec{b}$ and $\hat{k}||\vec{c}$. However, since we did our experiment on the same crystal in two different orientations, the spectrum differences we observed should come from the orientation dependence of the vibrational modes. Our experimental data are in line with the

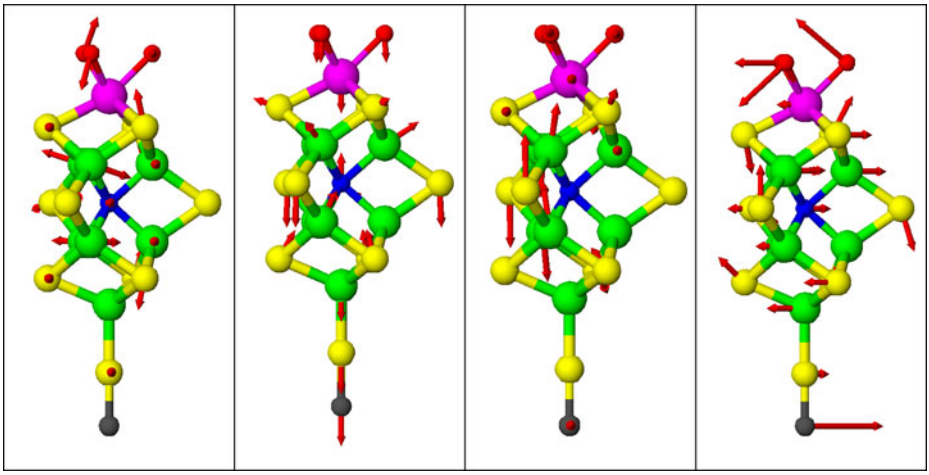

Fig. 6 Illustration of molecular motion in FeMo cofactor normal modes, derived from the normal mode calculation using a C_{3v} symmetry $[O_3MoFe_7NS_9(SC)]^{n-}$ FeMo cofactor model (2). Color code: Fe (*green*), S (*yellow*), Mo (*magenta*), O (*red*), C (*black*). *Left* to *right*: at 188, 177, 141, and 78 cm^{-1}. Figures were made with ATOMS

predicted spectra shown in Fig. 5. In the case of $\hat{k}||\vec{c}$ NRVS, all the C_3 axes of FeMo-co clusters are more aligned with the incident x-ray, and a decrease of intensity at $\sim$190 cm^{-1} and the increase at $\sim$148 cm^{-1} were observed . This behavior is consistent with the predicted spectrum shown in Fig. 5 when C_3 axis is aligned with the x-ray direction. Despite their limitations, the current spectra have already shown that single crystal NRVS is a promising technique to selectively probe vibrations from Fe sites even for complicated systems such as N_2ase.

4 Summary

In this work, we have investigated the combined application of single crystal EXAFS and single crystal NRVS on biological Fe-S centers. In the case of rubredoxin, the single crystal EXAFS spectra revealed an Fe-S bond length difference of $\sim$0.02 Å that cannot be resolved in solution data. In the *Pf* Rd crystal NRVS spectra, a 375 cm^{-1} mode had more intensity in the $\hat{k}||\vec{a}$ spectrum, corresponding to the shorter bonds seen by EXAFS.

In the MoFe protein crystal NRVS experiment, a multi-crystal MoFe protein was used. The crystal contained more than one single crystal with these sub crystals roughly aligned with each other. In a $\hat{k}||\vec{c}$ *vs.* $\hat{k}\perp\vec{c}$ spectral comparison, significant intensity differences can be seen. Using the simulation result from our previous MoFe protein NRVS studies on the frozen solution samples, we can explain these differences based on the different orientations of the Fe motions in the normal modes located at $\sim$150 and $\sim$190 cm^{-1}. Further experiments with additional orientations and using ^{57}Fe enriched FeMo cofactor MoFe protein single crystals would allow for more detailed analyses.

In summary, single crystal NRVS and EXAFS provide a powerful way to selectively probe the Fe centers of metalloproteins. The information obtained from experiments on crystals can help the interpretation of the corresponding frozen solution sample spectra in complicated protein systems. As synchrotron brightness continues to increase, the size of the requisite protein crystals will continue to diminish and the quality of the data will continue to improve.

Acknowledgements This work was funded by NIH GM-65440 (SPC), EB-001962 (SPC), the DOE Office of Biological and Environmental Research (SPC) and the DOE Office of Basic Energy Sciences (MWWA) Use of the APS is supported by the 334 DOE Office of Basic Energy Sciences. The experiments at SPring-8 were performed with the approval of Japan Synchrotron Radiation Research Institute. (Proposal No.: 2010B0032 - 2012A0032).

References

1. Johnson, D.C., Dean, D.R., Smith, A.D., Johnson, M.K.: Structure, function, and formation of biological iron-sulfur clusters. Ann. Rev. Biochem. **74**, 247–281 (2005)
2. Bau, R., Rees, D.C., Kurtz, D.M., Scott, R.A., Huang, H.S., Adams, M.W.W., Eidsness, M.K.: Crystal structure of rubredoxin from *Pyrococcus furiosus* at 0.95 Å resolution, and the structures of N-terminal methionine and formylmethionine variants of Pf Rd. Contributions of N-terminal interactions to thermostability. J. Biol. Inorg. Chem. **3**, 484–493 (1998)
3. Xiao, Y., Fisher, K., Smith, M.C., Newton, W., Case, D.A., George, S.J., Wang, H., Sturhahn, W., Alp, E.E., Zhao, J., Yoda, Y., Cramer, S.P.: How nitrogenase shakes—initial Information about P-cluster and FeMo-cofactor normal modes from nuclear resonance vibrational spectroscopy (NRVS). J. Am. Chem. Soc. **128**, 7608–7612 (2006)
4. Bergmann, U., Sturhahn, W., Linn, D.E., Jenney Jr., F.E., Adams, M.W.W., Rupnik, K., Hales, B.J., Alp, E.E., Mayse, A., Cramer, S.P.: Observation of Fe-H/D modes by nuclear resonant vibrational spectroscopy. J. Am. Chem. Soc. **125**, 4016–4017 (2003)
5. Xiao, Y., Wang, H., George, S.J., Smith, M.C., Adams, M.W.W., Francis, E., Jenney, J., Sturhahn, W., Alp, E.E., Zhao, J., Yoda, Y., Dey, A., Solomon, E.I., Cramer, S.P.: Normal mode analysis of *Pyrococcus furiosus* rubredoxin via nuclear resonant vibrational spectroscopy (NRVS) and resonance Raman spectroscopy. J. Am. Chem. Soc. **127**, 14596–14606 (2005)
6. Guo, Y., Wang, H., Xiao, Y., Vogt, S., Thauer, R.K., Shima, S., Volkers, P.I., Rauchfuss, T.B., Pelmenschikov, V., Case, D.A., Alp, E., Sturhahn, W., Yoda, Y., Cramer, S.P.: Characterization of the Fe site in iron-sulfur cluster-free hydrogenase (Hmd) and of a model compound via nuclear resonant vibrational spectroscopy (NRVS). Inorg. Chem. **47**, 3969–3977 (2008)
7. Xiao, Y., Tan, M.-L., Ichiye, T., Wang, H., Guo, Y., Smith, M.C., Meyer, J., Sturhahn, W., Alp, E.E., Zhao, J., Yoda, Y., Cramer, S.P.: Dynamics of *Rhodobacter capsulatus* [2Fe-2S] Ferredoxin VI and Aquifex aeolicus Ferredoxin 5 via nuclear resonance vibrational spectroscopy (NRVS) and resonance Raman spectroscopy. Biochemistry **47**, 6612–6627 (2008)
8. George, S.J., Igarashi, R.Y., Xiao, Y., Hernandez, J.A., Demuez, M., Zhao, D., Yoda, Y., Ludden, P.W., Rubio, L.M., Cramer, S.P.: EXAFS and NRVS reveal that NifB-co, a FeMo-co precursor, comprises a 6Fe Core with an interstitial light atom. J. Am. Chem. Soc. **130**, 5673–5680 (2008)
9. Sage, J.T., Durbin, S.M., Sturhahn, W., Wharton, D.C., Champion, P.M., Hession, P., Sutter, J., Alp, E.E.: Long-range reactive dynamics in myoglobin. Phys. Rev. Lett. **86**, 4966–4969 (2001)
10. Zeng, W.Q., Silvernail, N.J., Wharton, D.C., Georgiev, G.Y., Leu, B.M., Scheidt, W.R., Zhao, J.Y., Sturhahn, W., Alp, E.E., Sage, J.T.: Direct probe of iron vibrations elucidates NO activation of heme proteins. J. Am. Chem. Soc. **127**, 11200–11201 (2005)
11. Zeng, W., Barabanschikov, A., Zhang, Y., Zhao, J., Sturhahn, W., Alp, E.E., Sage, J.T.: Synchrotron-derived vibrational data confirm unprotonated oxo ligand in myoglobin compound II. J. Am. Chem. Soc. **130**, 1816 (2008)
12. Leu, B.M., Ching, T.H., Zhao, J.Y., Sturhahn, W., Alp, E.E., Sage, J.T.: Vibrational dynamics of iron in cytochrome c. J. Phys. Chem. B **113**, 2193–2200 (2009)

13. Krugh, T.R., Wittlin, F.N., Cramer, S.P.: Ethidium bromide—dinucleotide complexes, evidence for intercalation and sequence preferences in binding to double-stranded nucleic acids. Biopolymers **14**, 197–210 (1975)
14. Smith, M.C., Xiao, Y., Wang, H., George, S.J., Coucovanis, D., Koutmos, M., Sturhahn, W., Alp, E.E., Zhao, J., Cramer, S.P.: Normal mode analysis of $[FeCl_4]^-$ and $[Fe_2S_2Cl_4]^{2-}$ via vibrational mössbauer, resonance Raman, and FT-IR spectroscopy. Inorg. Chem. **44**, 5562–5570 (2005)
15. Xiao, Y., Koutmos, M., Case, D.A., Coucouvanis, D., Wang, H., Cramer, S.P.: Dynamics of an $[Fe_4S_4(SPh)_4]^{2-}$ cluster explored via IR, Raman, and nuclear resonance vibrational spectroscopy (NRVS)—analysis using ^{36}S su bstitution, DFT calculations, and empirical force fields. Dalton Trans. **18**, 2192–2201 (2006)
16. George, S.J., Igarashi, R.Y., Xiao, Y., Hernandez, J.A., Demuez, M., Zhao, D., Yoda, Y., Ludden, P.W., Rubio, L.M., Cramer, S.P.: Extended x-ray absorption fine structure and nuclear resonance vibrational Spectroscopy reveal that NifB-co, a FeMo-co precursor, comprises a 6Fe core with an interstitial light atom. J. Am. Chem. Soc. **130**, 5673–5680 (2008)
17. Bell, C.B., Wong, S.D., Xiao, Y.M., Klinker, E.J., Tenderholt, A.L., Smith, M.C., Rohde, J.U., Que, L., Cramer, S.P., Solomon, E.I.: A combined NRVS and DFT study of Fe-IV=O model complexes: a diagnostic method for the elucidation of non-heme iron enzyme intermediates. Angew. Chem. Int. Ed. **47**, 9071–9074 (2008)
18. Sage, J.T., Paxson, C., Wyllie, G.R.A., Sturhahn, W., Durbin, S.M., Champion, P.M., Alp, E.E., Scheidt, W.R.: Nuclear resonance vibrational spectroscopy of a protein active-site mimic. J. Phys.: Condens. Matter **13**, 7707–7722 (2001)
19. Rai, B.K., Durbin, S.M., Prohofsky, E.W., Sage, J.T., Ellison, M.K., Scheidt, W.R., Sturhahn, W., Alp, E.E.: Iron normal mode dynamics in a porphyrin-imidazole model for deoxyheme proteins. Phys. Rev. E **66**, (2002)
20. Rai, B.K., Durbin, S.M., Prohofsky, E.W., Sage, J.T., Ellison, M.K., Roth, A., Scheidt, W.R., Sturhahn, W., Alp, E.E.: Direct determination of the complete set of iron normal modes in a porphyrin-imidazole model for carbonmonoxy-heme proteins: [Fe(TPP)(CO)(1-Melm)]. J. Am. Chem. Soc. **125**, 6927–6936 (2003)
21. Leu, B.M., Zgierski, M.Z., Wyllie, G.R.A., Scheidt, W.R., Sturhahn, W., Alp, E.E., Durbin, S.M., Sage, J.T.: Quantitative vibrational dynamics of iron in nitrosyl porphyrins. J. Am. Chem. Soc. **126**, 4211–4227 (2004)
22. Leu, B.M., Silvernail, N.J., Zgierski, M.Z., Wyllie, G.R.A., Ellison, M.K., Scheidt, W.R., Zhao, J.Y., Sturhahn, W., Alp, E.E., Sage, J.T.: Quantitative vibrational dynamics of iron in carbonyl porphyrins. Biophysical Journal **92**, 3764–3783 (2007)
23. Paulsen, H., Schunernann, V., Trautwein, A.X., Winkler, H.: Mossbauer studies of coordination compounds using synchrotron radiation. **249**, 255–272 (2005)
24. Winkler, H., Chumakov, A.I., Trautwein, A.X.: Nuclear resonant forward and nuclear inelastic scattering using synchrotron radiation for spin crossover systems. **235**, 137–152 (2004)
25. Alp, E., Sturhahn, W., Toellner, T.S., Zhao, J., Hu, M., Brown, D.E.: Vibrational dynamics studies by nuclear resonant inelastic x-ray scattering. Hyp. Interact. **144/145**, 3–20 (2002)
26. Sturhahn, W.: Nuclear resonant spectroscopy. J. Phys. Cond. Matt. **16**, S497–S530 (2004)
27. Sturhahn, W., Toellner, T.S., Alp, E.E., Zhang, X., Ando, M., Yoda, Y., Kikuta, S., Seto, M., Kimball, C.W., Dabrowski, B.: Phonon density of states measured by inelastic nuclear resonant scattering. Phys. Rev. Lett. **74**, 3832–3835 (1995)
28. Meyer, J., Moulis, J.-M.: Rubredoxin. In: Messerschmidt, A., Huber, R. (eds.) Handbook of Metalloproteins, vol. 1, pp. 505–517. Wiley, New York (2001)
29. Dauter, Z., Wilson, K.S., Sieker, L.C., Moulis, J.M., Meyer, J.: Zinc- and iron-rubredoxins from Clostridium pasteurianum at atomic resolution: a high-precision model of a ZnS4 coordination unit in a protein. Proc. Natl. Acad. Sci. U. S. A. **93**, 8836–8840 (1996)
30. Bonisch, H., Schmidt, C.L.: Ultrahigh-resolution study on *Pyrococcus abyssi* rubredoxin. I. 0.69 Å x-ray structure of mutant W4L/R5S. Acta Crystallogr. D **61**, 990–1004 (2005)
31. Jenney Jr., F.E., Adams, M.W.W.: Rubredoxin from *Pyrococcus furiosus*. Methods Enzymol. **334**, 45–55 (2001)
32. Ducruix, A., Giege, R.: In: Crystallization of Nucleic Acid and Proteins, p. 73. Oxford University Press, Oxford (1992)
33. Georgiadis, M.M., Komiya, H., Chakrabarti, P., Woo, D., Kornuc, J.J., Rees, D.C.: Crystallographic structure of the nitrogenase iron protein from *Azotobacter vinelandli*. Science **257**, 1653–1659 (1992)
34. Alp, E.E., Mooney, T.M., Toellner, T., Sturhahn, W.: Nuclear resonant scattering beamline at the advanced Photon Source. **90**, 323–334 (1994)

35. Yoda, Y., Yabashi, M., Izumi, K., Zhang, X.W., Kishimoto, S., Kitao, S., Seto, M., Mitsui, T., Harami, T., Imai, Y., Kikuta, S.: Nuclear resonant scattering beamline at SPring-8. Nucl. Instrum. Methods A **467**, 715–718 (2001)
36. Shape Software. http://www.shapesoftware.com/
37. Dowty, E.: Fully automated microcomputer calculation of vibrational spectra. Phys. Chem. Miner. **14**, 67–79 (1987)
38. Engeln-Mueller, G., Uhlig, F.: Numerical Algorithms with C. Springer, Berlin (1996)
39. EXAFSPAK: a Suite of Computer Programs for Analysis of x-ray Absorption Spectra. http://ssrl.slac.stanford.edu/exafspak.html
40. Rehr, J.J., Albers, R.C.: Theoretical approaches to x-ray absorption fine structure. Rev. Mod. Phys. **72**, 621–654 (2000)